SCIENTIFIC REPORTS

OPEN

SUBJECT AREAS:
BIOINSPIRED MATERIALS
EXTRACELLULAR SIGNALLING MOLECULES

Received
28 May 2014

Accepted
28 August 2014

Published
19 September 2014

Correspondence and requests for materials should be addressed to A.J.E. (aengler@ucsd.edu)

Mechanosensitive Kinases Regulate Stiffness-Induced Cardiomyocyte Maturation

Jennifer L. Young[1], Kyle Kretchmer[1], Matthew G. Ondeck[3], Alexander C. Zambon[2] & Adam J. Engler[1,3,4]

[1]Department of Bioengineering, University of California, San Diego, CA 92093, [2]Department of Pharmacology, University of California, San Diego, CA 92093, [3]Department of Material Science Program, University of California, San Diego, CA 92093, [4]Sanford Consortium for Regenerative Medicine, La Jolla, CA 92037.

Cells secrete and assemble extracellular matrix throughout development, giving rise to time-dependent, tissue-specific stiffness. Mimicking myocardial matrix stiffening, i.e. ~10-fold increase over 1 week, with a hydrogel system enhances myofibrillar organization of embryonic cardiomyocytes compared to static hydrogels, and thus we sought to identify specific mechanosensitive proteins involved. Expression and/or phosphorylation state of 309 unique protein kinases were examined in embryonic cardiomyocytes plated on either dynamically stiffening or static mature myocardial stiffness hydrogels. Gene ontology analysis of these kinases identified cardiogenic pathways that exhibited time-dependent up-regulation on dynamic versus static matrices, including PI3K/AKT and p38 MAPK, while GSK3β, a known antagonist of cardiomyocyte maturation, was down-regulated. Additionally, inhibiting GSK3β on static matrices improved spontaneous contraction and myofibril organization, while inhibiting agonist AKT on dynamic matrices reduced myofibril organization and spontaneous contraction, confirming its role in mechanically-driven maturation. Together, these data indicate that mechanically-driven maturation is at least partially achieved via active mechanosensing at focal adhesions, affecting expression and phosphorylation of a variety of protein kinases important to cardiomyogenesis.

Extracellular matrix (ECM) elasticity, or 'stiffness' (measured in Pascal, Pa), regulates a variety of signaling pathways and subsequent cellular responses, e.g. differentiation[1,2], via myosin-based contractility[3]. These pathways, e.g. p130CAS-Rap1[4], likely undergo significant temporal regulation throughout development as cells secrete and assemble ECM[5], giving rise to stiffer, mature tissues[6,7]. Stiffer matrices require increased contractile work for cells to deform their surrounding microenvironment. The increased work done by cells is borne out from changes in mechanosensitive signaling pathways[3], such as with cardiomyocytes plated on stiffer substrates requiring more myosin II contractility[1,2,8]. While aberrantly stiff matrix, i.e. as in tissue fibrosis, can impair myosin II function *in vitro*[9], we hypothesized that providing *in vivo*-like changes in stiffness found during development would enhance cardiomyoycte sarcomere organization and calcium handling. Static substrate stiffness is known to influence migration[10,11], adhesion[12,13], proliferation[14,15], and differentiation[1,2], but temporal changes in stiffness that mirror *in vivo* stiffening are known to impact the expression of cardiac markers and sarcomere assembly[16]. When these behaviors are integrated over many cells, stiffening can affect tissue morphogenesis[6,17], e.g. tubulogenesis[18] and heart development[19], making stiffness not just a significant niche component, but one that must be appropriately mimicked over time *in vitro*.

Temporal changes are likely important in almost every developmental context, but they are especially important for cardiomyocytes, which contract more effectively when grown on substrates mimicking the stiffness of their native microenvironment versus rigid substrates[16,20]. Improved contractility in mature cardiomyocytes may be due in part to the modulation of myofibril organization and alignment, both of which can affect beating rate, and are known to be regulated by matrix stiffness[8,9]. On a hydrogel of 10 kiloPascal (kPa), which approximates the adult myocardium[21], intra- and extracellular strains become matched in mature cardiomyocytes, thereby prolonging rhythmic beating in culture compared to substrates that are too soft or stiff[9]. Despite improved mature cardiomyocyte function on matrices with biomimetic stiffness, the heart does not begin as a contractile ~10 kPa ECM but instead originates from much softer mesoderm where stiffness is less than 500 Pa[16,22,23] and stiffens up to 10 kPa by embryonic day 14 with a $\tau_{1/2} \sim 60$ hr[16]. Mimicking myocardial stiffening dynamics using a thiolated hyaluronic acid (HA-SH)/poly(ethylene glycol) diacrylate (PEGDA) hydrogel, stiffening from ~2 to

9 kPa with $\tau_{1/2} \sim 69$ hr in the absence of specific exogenous growth factors aside from serum, resulted in improved cardiomyocyte maturation based on gene expression and myofibrillar assembly[16].

Many of the same signaling pathways for static matrices may be relevant for dynamic ones, but those most relevant to cardiac maturation are likely to be critical spatiotemporal heart patterning pathways[24,25]. Such pathways include agonist phosphatidylinositol 3-kinase (PI3K)/protein kinase B (PKB/AKT)[26,27] and non-canonical *Wnt*/Ca^{28} and *Wnt*/polarity pathways[29], as well as the antagonist canonical *Wnt*/β-catenin pathway, which acts via GSK-3β, among other important targets[30,31]. While these signaling pathways have been extensively studied and identified as major regulators of cardiac development and differentiation both *in vitro* and/or *in vivo*, stiffness-mediated activation remains unclear. To understand what role these and other pathways play in regulating sarcomere organization and calcium handling in maturing embryonic cardiomyocytes, a systematic examination of protein kinase pathway activation with respect to dynamic vs. static substrate stiffness was conducted.

Results

Stiffness-mediated sarcomere assembly. To examine how dynamic vs. static stiffness affects cardiomyocytes, pre-cardiac mesodermal cells were cultured *in vitro* on polyacrylamide (PA) hydrogels of 1, 11, and 34 kPa whose stiffness did not change with time and were thus 'static.' Cells were also plated on hyaluronic acid (HA) hydrogels, whose stiffness changed from ~2 to 8 kPa (τ = 69.9 hr) or ~0.2 to 5 kPa ($\tau \gg 100$ hr) over one week in culture depending on the use of high (HMW) or low molecular weight (LMW) PEGDA crosslinker, respectively[16], to make HA hydrogels appear 'dynamic'. After 1 and 11 days (96 and 336 HPF, respectively) in culture, cells on 1 kPa static matrices were either rounded and/or exhibited poor myofibril development independent of time (Fig. 1, first row). On stiff substrates similar to a fibrotic niche[21], e.g. 34 kPa static hydrogel, cells quickly developed a rod-shaped morphology but a dominant fraction formed syncytia over the time course (Fig. 1, third row). Cell changes within clusters could result from both cell-matrix and cell-cell effects and thus were omitted from further analysis. For static 11 kPa PA hydrogels and both dynamic HA hydrogels, cells developed a rod-shaped morphology over time with the highest percentage of striated single cells (Fig. 1, second, fourth, and fifth rows). Despite similar morphology, isolated myocytes on HMW PEGDA/HA hydrogels developed myofibrils over time with average z-disc spacing of 1.8 μm (Fig. 2A, blue), which is indicative of mature myofibrils[32]. Myocytes on less dynamic LMW PEGDA/HA hydrogels and static 11 kPa hydrogels, however, exhibited a significant population of cells with immature sarcomeres, indicated by lower z-disc spacing (<1.8 μm[32]; Fig. 2A, orange and green, respectively). Myocytes on the softest or stiffest substrates were excluded from measurement because a majority of cells did not exhibit striations or were obscured by fibroblast proliferation and the prevalence of cell-cell junctions (Fig. 1).

To determine if sarcomere assembly differences resulted in functional changes, calcium transients, which regulate contraction magnitude and duration[33], were observed for isolated myocytes (Supplemental Video 1). To better quantify these transients, a power spectral density (PSD) was computed, both overall and as a function of beat frequency to indicate contraction regularity[34]. Over the duration of stiffening, average maximal PSD remained relatively constant on static 11 kPa PA hydrogels and both dynamic HA hydrogels (Fig. 2B). However as a function of beating frequency, dominant peaks at regular intervals were present for all substrates initially after plating, but over time, power spectrum peaks on dynamic HMW PEGDA/HA hydrogels maintained their periodicity (Fig. 2C, top) whereas peaks on less dynamic LMW PEGDA/HA hydrogels and static PA hydrogels were sporadic (Fig. 2C, middle and bottom, respectively). Together, these data indicate that matrices that are too soft or stiff relative to mature niche stiffness, e.g. 10 kPa[8,9,16], impair sarcomere assembly and calcium handling. This data also indicates that presenting mature matrix stiffness to immature cells for a tissue in which the cells normally develop can also adversely affect maturation of those precursor cells. While signaling events regulating development and myofilament assembly may be fairly well described *in vivo*[35,36], the specific contributions of dynamic matrix stiffness remain uncertain but could be teased out using the matrices described here.

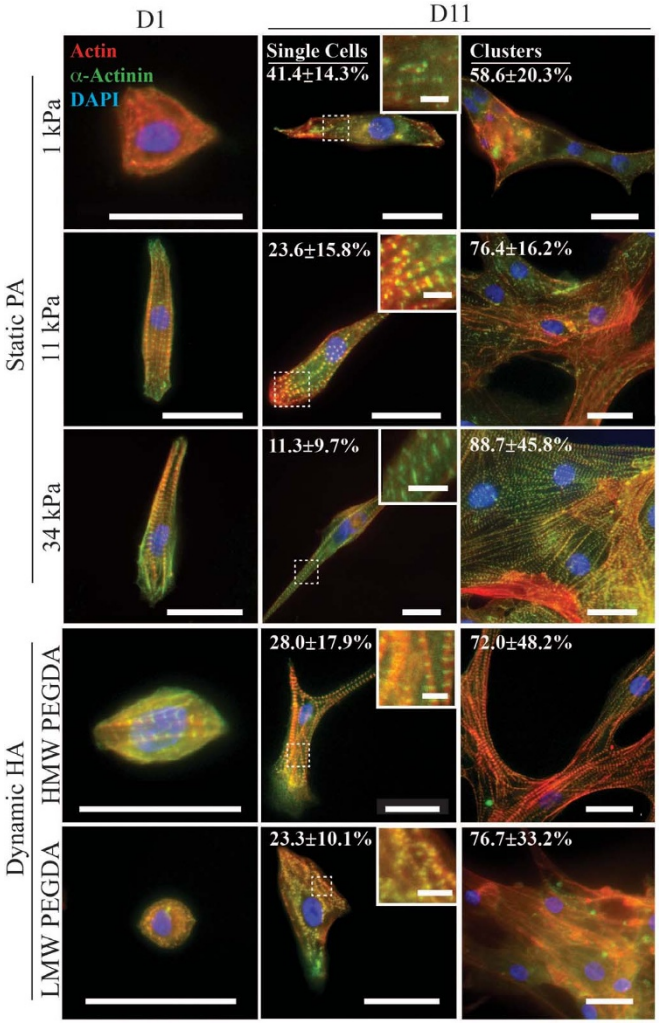

Figure 1 | Sarcomere Assembly on Hydrogels Improves with Dynamic Stiffening. Immunofluorescence of α-actinin (green), actin (red) and nuclei (blue) for 72 HPF cardiomyocytes at 1 (D1) and 11 (D11) days after plating on static 1 kPa (first row), 11 kPa (second row) and 34 kPa (third row) PA hydrogels and on dynamic HA hydrogels crosslinked using HMW PEGDA (fourth row) and of LMW PEDGA (fifth row). Day 11 images consist of single cells (middle column, inset indicated by white dashed box) and clustered cells (right column) where the indicated percentage corresponds to the fraction of cardiomyocytes in that state, i.e. single or clusters of cells, with error shown from technical replicates. Dashed boxes indicate where the inset images were taken. Scale bars = 25 μm for large images and 3 μm for insets.

Mechanosensitive signaling. A protein kinase microarray was employed to compare signaling differences in 72 HPF embryonic cardiomyocytes plated on the most dynamic hydrogel, i.e. HMW PEGDA/HA, and static 11 kPa PA hydrogels for 1, 3, 5 and 11 days (for a total age of 96, 144, 192 and 336 HPF, respectively), as myocardial development and stiffening conclude by ~336 HPF[16,37].

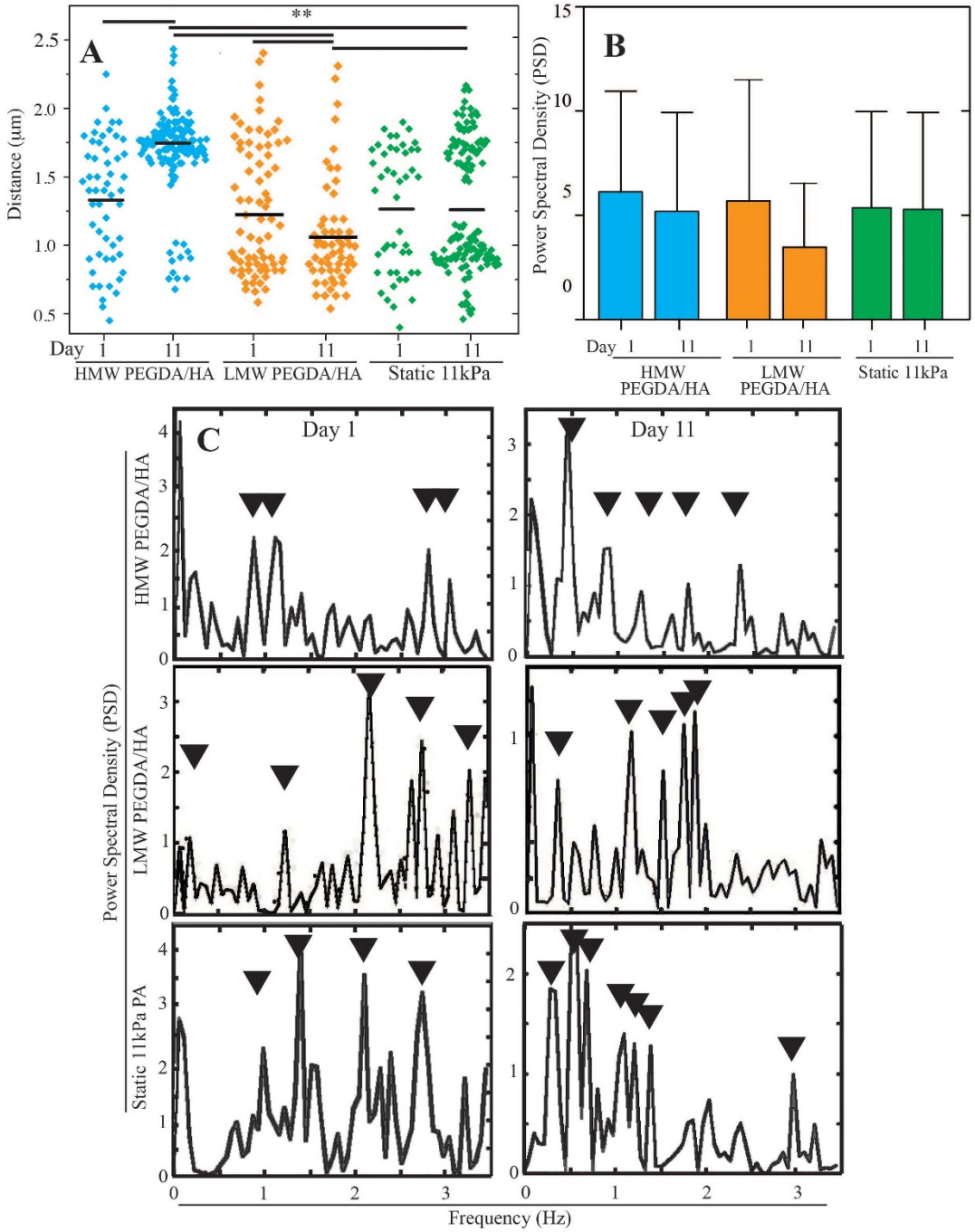

Figure 2 | Myofibril Development and Calcium Imaging of Static and Dynamic Hydrogels. (A) Sarcomere spacing (μm) of individual myofibrils was plotted for HMW PEGDA/HA (blue), LMW PEGDA/HA (orange) and static 11 kPa PA (green) hydrogels at 1 and 11 days after plating. The number of cells and myofibrils analyzed exceed 12 and range between 50 and 150, respectively. $^{**}p < 0.01$. (B) Average maximal power spectral density (PSD) of beating from calcium imaging was plotted for cells 1 and 11 days after plating on HMW PEGDA/HA, LMW PEGDA/HA, and static 11 kPa PA hydrogels. Error bars indicate standard deviation. (C) Power spectral density (PSD) plotted vs. frequency was shown 1 (left) and 11 days (right) after plating 72 HPF cardiomyocytes on HMW PEGDA/HA (top), LMW PEGDA/HA (middle) and static 11 kPa PA (bottom) hydrogels. Peaks in the power spectrum are indicated by arrowheads; graphs are representative analyses of single cells.

While this sampling rate is relatively low for kinase screens, it was intended to capture changes from as much of the stiffening dynamics as possible; sampling at higher rates may limit data quality over the entire 336-hour duration of stiffening. Data collected at these time points was normalized to the initial post-isolation time point, and expression of 280 phosphorylated and 530 pan-specific proteins were assessed. 255 unique proteins measures were found to have statistically significant changes in expression or phosphorylation over time and between hydrogels types based on 2-way ANOVA analysis of their z-ratios. In order to convey greater differences in the data for the purpose of clustering and identifying important proteins, data was further filtered to only include proteins exhibiting at least one z-ratio of greater than 1 or less than −1, of which 199 unique proteins were identified (Supplemental Table 1). As shown in Figure 3 and annotated in Supplement Table 1, data was grouped based on z-ratio where time increases to the right, and data from dynamic HMW

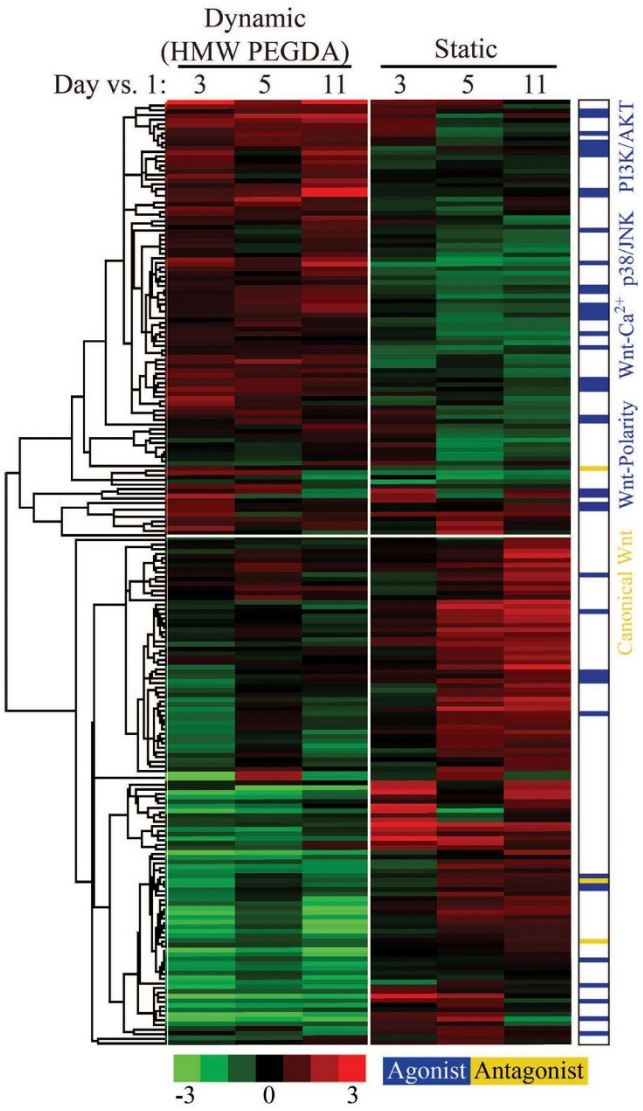

Figure 3 | Microarray Data Clustering Reveals Differentially Expressed Protein Kinases on Dynamic versus Static Hydrogels. Z-ratios of differentially expressed (at least one z-ratio > 1 or < -1) significant data (interaction $p < 0.05$) of dynamic HMW PEGDA/HA and static 11 kPa PA hydrogels over 3, 5 and 11 days in culture compared to cells initially isolated cultured for 1 day were clustered using centroid gene clustering linkages. Z-ratios range from a down regulation value of −3 (green), to no change (0; black) to an up-regulation value of +3 (red) versus global expression. At the right side of the figure, agonists of cardiac development (e.g. Wnt-Polarity, Wnt-Ca^{2+}, p38/JNK, PI3K/AKT) were highlighted in blue while antagonists (e.g. Wnt-Canonical) were highlighted in yellow.

PEGDA/HA and static 11 kPa PA hydrogels are on the left and right portions of the heat map, respectively. 90 and 109 proteins were differentially expressed in myocytes on dynamic HA and static PA hydrogels, respectively. When annotating the role of these proteins as cardiac developmental agonists (blue; e.g. PI3K/AKT, Wnt-Ca^{2+}, Wnt-Polarity and p38/JNK pathways) or antagonists (yellow; e.g. canonical Wnt signaling)[24,25], we found that 25 out of 90 proteins (27%) were differentially up-regulated in myocytes on dynamic HMW PEGDA/HA matrices over time versus only 14 out of 109 (13%) for static PA matrices. More antagonists were also up-regulated on static PA vs. dynamic HMW PEGDA/HA matrices (right hand column, Fig. 3). Agonist expression (blue) also generally increased with time, and thereby stiffness, on dynamic HMW PEGDA/HA hydrogels, with a corresponding decrease in antagonist (yellow) expression with time and stiffness, resulting in a correlation coefficient of −0.53 (Fig. S1, top). Conversely, antagonist expression was positively correlated with agonist expression (coefficient of 0.91) on static PA hydrogels (Fig. S1, bottom), indicating that time-dependent mechanical cues likely affect protein function.

While agonist/antagonist annotation indicated general signaling differences, gene ontology (GO) analysis[38,39] was used to identify important pathways utilizing all proteins but noting the 255 statistically significant proteins. Among all pathways within the GO-ELITE program, the focal adhesion signaling Wikipathway, which encompasses PI3K/AKT, Wnt signaling, and p38 MAPK/JNK cardiac pathways[24,25], contained the greatest percentage of differentially expressed or phosphorylated proteins (Fig. 4). More specifically, the PI3K/AKT pathway, which plays a major role in regulating survival, proliferation, growth, regeneration and metabolism of cardiomyocytes[40], was differentially expressed. During development, AKT regulates cardiogenesis through various downstream targets, e.g. inhibition of the cardiogenesis antagonist GSK3β[41]. Here, GO clustering indicated AKT was highly up-regulated on dynamic HMW PEGDA/HA hydrogels vs. static 11 kPa PA hydrogels. Corresponding down-regulation of GSK3β on dynamic HMW PEGDA/HA hydrogels vs. static 11 kPa PA hydrogels was also observed (Fig. S2A). These data were consistent across many antibodies within the array and illustrate proteins within these pathways that change significantly between systems and with time, e.g. AKT1/2 and GSK3β. However, a number of focal adhesion proteins that have been previously implicated in mechanotransduction[42,43] had many more antibodies that did not change as a function of time and/or material than AKT and GSK3β, e.g. paxillin (Fig. S2A, yellow data; Fig. S2B). Together, these data imply that agonist pathways have higher expression in developing myocytes on dynamic hydrogels, while antagonist pathway expression was greater on static hydrogels.

Western blot analysis confirmed expression of specific proteins within these pathways as only antibodies for total expression rather than specific phosphorylation site were available (Fig. S3A, C); for example, we observed enhanced expression of AKT 1 and AKT 2 on dynamic HMW PEGDA/HA (dark grey) vs. static PA (light grey) in both methods, as well as enhanced expression of the antagonist GSK3β on static PA hydrogels. Focal adhesion protein expression was higher for static PA than dynamic HMW PEGDA/HA hydrogels, e.g. paxillin (Fig. S3A, C), as has been shown for cells plated on stiffer substrates[44,45]. Conversely, array data only showed significant differences for phosphorylation sites and not for total expression (Fig. 4, Supplemental Table 1). Despite other proteins being less correlated, critical signaling cascades identified by GO, e.g. AKT which inhibits GSK3β expression[24], appear robust and could be corroborated (Fig. S3A, C) with array data (Fig. 3 and 4).

Comparison with parallel maturation *in vivo* was also performed to provide a more complete assessment of *in vitro* cell state. Western blotting of embryonic myocardium 72, 120, 144, 240 and 288 HFP indicated that paxillin and AKT 1 but not AKT 2 and GSK3β expression increased (Fig. S3B, D). Direct comparisons of mature *in vivo* expression to age-matched myocytes cultured on the hydrogels showed that cells that matured on dynamic HMW PEGDA/HA hydrogels (dark gray bars) were similar to cells that matured in the animal for AKT1/2 and GSK3β as indicated by western blotting (Fig. 5A) and microarray (Fig. 5B). Conversely, GSK3β was up-regulated and AKT1/2 was down-regulated for cells on static hydrogels relative to *in vivo* controls (light gray bars, Fig. 5). These data imply a correlation in AKT1/2 and GSK3β expression for blotting and arrays vs. *in vivo* at least for the signals that are upregulated on a particular hydrogel, e.g. AKT1/2 and HMW PEGDA/HA hydrogels.

Assessing downstream signaling affected by time-dependent stiffening. To functionally assess the effects of AKT1/2 and GSK3β on time-dependent stiffness-induced sarcomere assembly and calcium

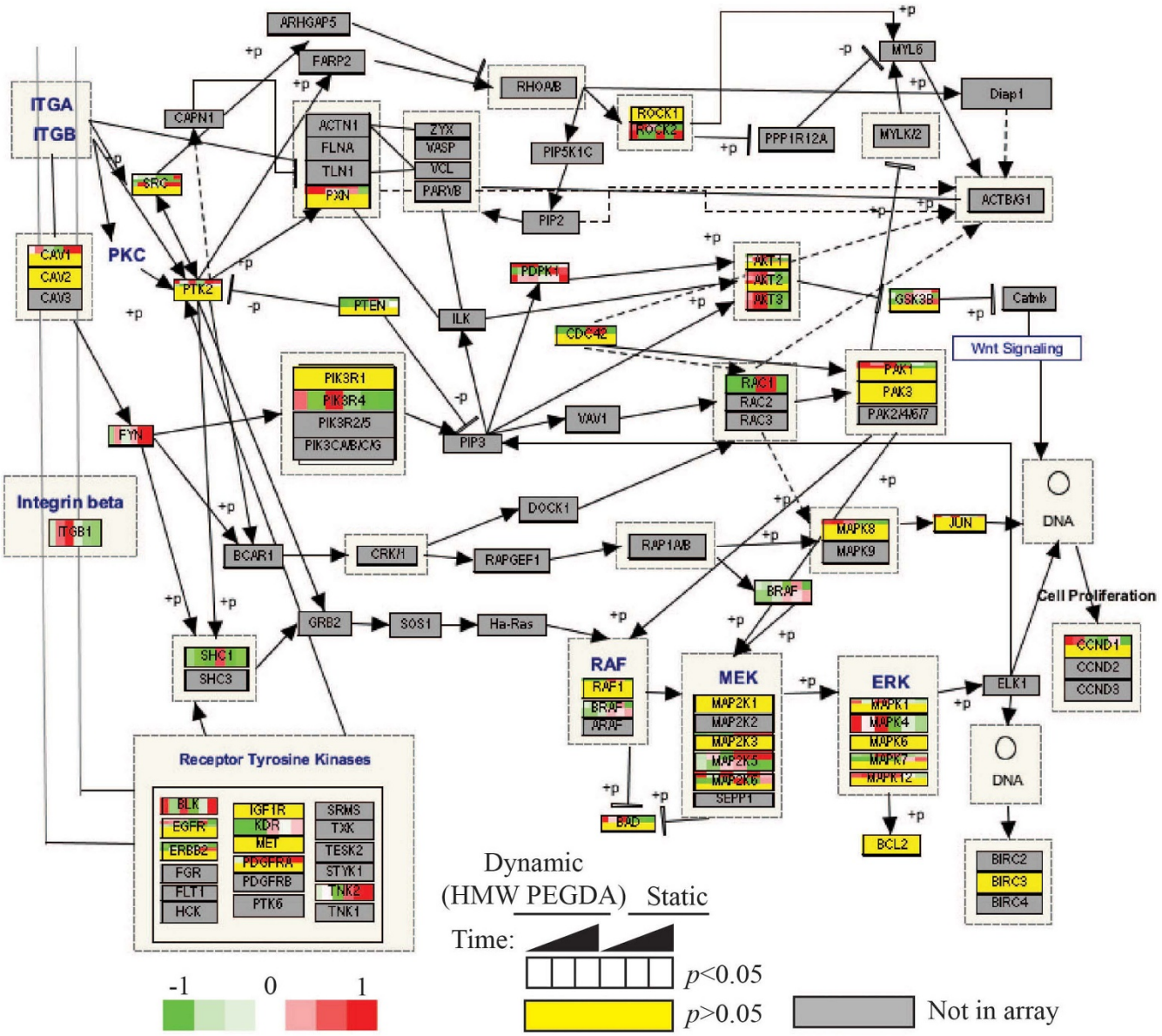

Figure 4 | Focal Adhesion Signaling is Substrate Stiffness-Dependent. Focal Adhesion Signaling WikiPathway, identified by GO-ELITE analysis of the microarray data, is shown in a more complete annotation of Fig. S2. For genes with interaction $p < 0.05$, protein boxes were divided into 6 smaller boxes indicating z-ratios from 3, 5 and 11 days in culture compared to cells initially isolated cultured for 1 day (left to right) for dynamic HMW PEGDA/HA (left three boxes) and static 11 kPa PA (right three boxes). Rows within each box indicate different antibodies used for each target. For proteins with interaction $p > 0.05$, boxes were shaded yellow. For proteins not included in the array, the protein boxes are shaded grey. The color map indicates down-regulation (−1, green), no change with respect to the global average (0, white) and up-regulation (+1, red).

handling, AKT1/2 and GSK3β were inhibited via the addition of MK-2206[46] and CHIR-99021[47], respectively. In addition to functional inhibition, both also significantly reduced expression as observed via western blot (Fig. 6A). When AKT1/2 was inhibited, myofibril development over time was impaired on HMW PEGDA/HA hydrogels relative to DMSO controls (Fig. 6B, top left vs. right), resulting in some fibrils exhibiting extremely short sarcomere spacing (Fig. 6C). Conversely, GSK3β inhibition resulted in improved formation of myofibrils over time on static PA hydrogels (Fig. 6B, bottom center vs. right, Fig. 6C). A similar trend was observed for calcium transients where PSD increased on static PA hydrogels when GSK3β is inhibited but decreased for dynamic HMW PEGDA/HA hydrogels when AKT1/2 was inhibited (Fig. 6D; Supplemental Video 2). As illustrated in Fig. S2, AKT inhibits GSK3β expression[24] and this can regulate Wnt signaling via β-catenin[69]. In dynamic HMW PEGDA/HA but not in less dynamic LMW PEGDA/HA or static PA hydrogels, β-catenin localized to the nucleus over time. Inhibition of AKT1/2, but not GSK3β, also blocked β-catenin localization (Fig. 7), further indicating that dynamic HMW PEGDA/HA hydrogels mechanically induce sarcomere formation and regulate calcium handling via AKT and possibly Wnts.

Discussion

While there is a developing appreciation for the role that mechanics can play along with growth factors in stem cell differentiation, our understanding of the molecular mechanisms of this process, let alone in an *in vitro* environment that can signal to cells from its dynamic properties, is somewhat limited. To address this problem, we identified a direct link between dynamic matrix mechanics and specific signal transduction pathways that regulate cardiogenesis. Our data

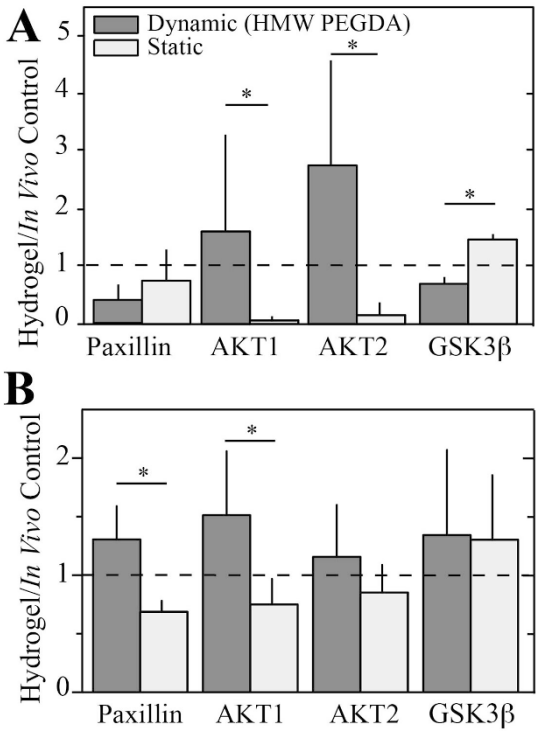

Figure 5 | Maturation of Cells In Vitro vs. In Vivo as Assessed by Western Blot and Microarray. (A) Ratio of paxillin (PXN), AKT 1, AKT 2 and GSK3β expression in cells isolated 72 HPF and cultured for 11 days on dynamic HMW PEGDA/HA (dark grey) and static 11 kPa PA (light grey) to time-matched chicken lysate control samples (336 HPF) as determined by western blot analysis. Dashed line indicates a ratio of 1.
(B) Corresponding ratios from microarray data. $*p < 0.05$.

shows that the presentation of developmentally-relevant tissue mechanics can enhance cardiomyocyte maturation and function in culture, consequently leading to the activation of protein kinases required for proper development. When presented with static matrices, maturation is hindered in immature cardiomyocytes, leading to an up-regulation of antagonistic pathways of cardiogenesis. Using pathway antagonists, we showed that mechanically induced signaling can be altered to make permissive substrates appear non-permissive and vice versa. As the stiffening dynamics of our culture system here intentionally mirror mechanics of cardiac tissue morphogenesis, some of the signaling observations obtained from these mechanics alone directly mirror what has been previously found in development as we describe below. Also noted below are specific caveats to the culture system and the types of signals examined here.

Mechanosensing in development guides matrix design. Heart morphogenesis, as well as differentiation and development of resident cardiac cells, has been classically described by growth factor gradients[48–50], but can also be driven by active mechanical forces derived from torsion, bending, and fluid shear stress[51,52]. More recently, passive mechanical properties, e.g. Young's Modulus, have also been observed to assist in heart development and patterning[23,53]. Concomitant with these active mechanical and morphological events are changes in ECM composition, which can be up- or down-regulated as much as 10-fold[16,54]; misregulation of matrix proteins during cardiac development can stiffen tissues and induce a variety of defects[21,55]. Yet, as cells secrete and assemble new matrix under healthy conditions, passive mechanical properties gradually stiffen[16,19] and can induce cardiomyocyte lineage marker expression and sarcomere assembly[16].

As this occurs, how cells feel their environment changes, and if done so over an appropriate time period and within an appropriate stiffness range, mechanotransductive signaling can guide development and myofilament assembly[35]. However, increasing matrix stiffness beyond this point can negatively regulate cardiomyocyte maturation[9,56] and their calcium handling[8]. In agreement with these *in vivo* and *in vitro* data on the negative effects of improper stiffness on cardiomyocyte phenotype, our findings indicate that matrices that are too soft or stiff relative to the mature niche, i.e. ~10 kPa for muscle[1], impair maturation via decreased myofibril formation and contractility. Presenting a matrix of mature tissue stiffness to immature cells of that same tissue type can also adversely affect maturation, indicating the importance of reflecting the precise time-dependent characteristics of the constituent tissue. While this *in vitro* system is useful to isolate and examine the influence of specific bulk ECM characteristics on cells in 2D, it is also important to note its limitations; first multiple cell types comprise the cardiovascular system and secrete and assemble their own complex ECM, e.g. cardiac fibroblasts[57]. Even cardiomyocytes themselves secrete at least collagen IV, XVIII and fibronectin[58] and thus the dynamic control provided by the HA substrate with time is likely augmented by cell-mediated niche remodeling. A second important area of concern is the difference in mechanotransduction that could exist in a 3D environment versus the dynamic 2D system here. Indeed, cardiomyocytes in 3D matrices are smaller, form critical cell-cell junctions, and express different proteins[59]. Though they often have high cell density convoluting substrate effects, these 3D systems can reconstitute many maturation processes and signaling pathways found *in vivo* through a combination of matrix and junctional signaling[60]. Additionally, we noted some differences in protein regulation for adhesive proteins versus kinases when comparing *in vivo* to hydrogel system expression, e.g. paxillin vs. AKT1/2. While this may be expected given the limited number of cues presented to isolated cells in these assays, it certainly warrants a note of caution and further investigation. That said, reductionist systems such as the HA substrates here are becoming increasingly complex, and for signals that they recapitulate in developmentally appropriate ways, there is a surprising degree of control over cell behavior and maturation. It is also interesting that cells interpret these ECM changes using canonical pathways, which we will discuss below.

Matrix-dependent pathway analyses in maturing cardiomyocytes. Contractility has been shown to be critical for matrix-mediated differentiation, both *in vitro* and *in vivo*[9,61]; however the molecular links between ECM and cardiac differentiation are less appreciated; thus we chose to more closely examine intermediary effects, i.e. protein kinase signaling, on pre-cardiac mesodermal cells on substrates with dynamic vs. static stiffness. Precise spatial and temporal patterning of the heart is achieved partially through the activation of signal transduction pathways involving a highly complex network of interacting protein kinases, both positively- and negatively-acting on differentiation, e.g. p38 MAPK, PI3K/AKT, and Wnts[24,25]. That said, these previous studies in stem cells have almost exclusively been examined using chemical induction of these pathways, yet activation of specific pathways due to mechanical cues has been less studied. These cardiac signal transduction networks are extremely complex, and thus a protein kinase microarray was performed to identify global perturbations as a result of matrix stiffness alone. Gene clustering and ontology analysis identified that agonists of cardiogenesis were more highly up-regulated on dynamic HMW PEGDA/HA vs. static hydrogels, providing a molecular explanation for improved cardiomyocyte function. More specifically, the PI3K/AKT pathway, which plays a major role in regulating survival, proliferation, growth, regeneration and metabolism of cardiomyocytes[40], was differentially expressed. During development, AKT regulates cardiogenesis through various downstream targets, e.g. inhibition of antagonist of cardiogenesis, GSK3β[41]. Here, AKT was highly up-regulated, consistent across a

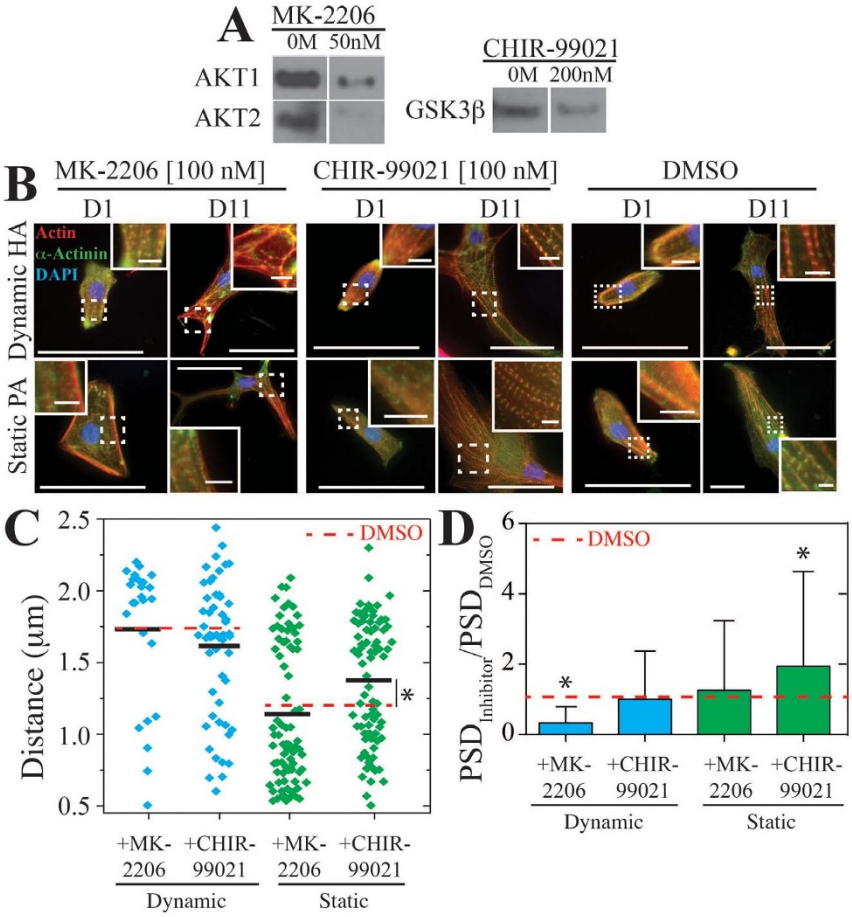

Figure 6 | Inhibition of Mechanosensitive Players Results in Appropriate Responses. (A) Western blots of MK-2206- (left) and CHIR-99021-treated cells (right) at their indicated concentrations. Data was normalized by total protein concentration as determined by BCA assay. (B) Representative fluorescent images of 72 HPF isolated chicken cardiomyocytes after 1 and 11 days on dynamic HMW PEGDA/HA (top) or static 11 kPa PA (bottom). Cells were cultured in the presence MK-2206 (100 nM), CHIR-99021 (100 nM), or DMSO as indicated. Dashed white boxes indicate the inset regions. Scale bars = 50 μm and 5 μm for insets. (C) Sarcomere spacing of individual myofibrils was plotted for dynamic HMW PEGDA/HA (blue) and static 11 kPa PA (green) hydrogels after 11 days in culture in the presence of MK-2206 or CHIR-99021 as indicated. A red-dashed line indicated the average for DMSO-treated cells. $*p < 0.05$ for comparisons to DMSO-treated cells. (D) The average power spectral density (PSD) of beating from calcium imaging was plotted as a ratio of the indicated inhibitor-treated cells to DMSO-treated cells. Cells cultured on dynamic HMW PEGDA/HA and static 11 kPa PA hydrogels at 11 days after plating are shown in blue and green, respectively. Cells were treated with either MK-2206 (left) or CHIR-99021 (right). Red-dashed line indicates a ratio of 1 or no change from DMSO-treated control cells. $*p < 0.05$ for comparisons to DMSO-treated cells.

panel of antibodies, on HMW PEGDA/HA vs. static hydrogels, corresponding with a down-regulation of GSK3β on HMW PEGDA/HA vs. static matrices. Furthermore, inhibition of GSK3β on static substrates resulted in enhanced myofibril assembly and function, while inhibition of AKT on HMW PEGDA/HA substrates decreased function, thereby demonstrating the importance of these two proteins in stiffness-mediated maturation. This data is also supported by β-catenin localization, in which nuclear translocation is present only in HMW PEGDA/HA with or without GSK3β inhibitor and static PA with AKT inhibitor. While these data and the microarrays suggest Wnt-dependent signaling as observed elsewhere for canonical Wnt signaling[62], β-catenin localization has also been shown to occur via Wnt-independent mechanism(s)[63]; thus the temporal stiffening-induced activation of AKT and localization of β-catenin that we detected may not specifically identify the type of downstream signaling that manifests in striation maturation and calcium handling.

Together, these data indicate that perturbing mechanosensitive signaling pathways can affect the ability of a cell to undergo stiffness-based maturation. These data could also be useful in cellular cardiomyoplasty, i.e. cells injected into the fibrotic tissue formed after a myocardial infarction improperly differentiate based on the diseased, stiff niche[64], as one could alter undesirable responses by inhibiting specific mechanosensitive pathways. Thus, in an infarct where matrix is stiffening with time, mechanosensitive maturation of injected cells may be controlled by independently manipulating AKT and GSK3β pathways. That said, these pathways could also be modulated by more complex extracellular changes with time in addition to stiffness such as tethering of the matrix proteins to the underlying hydrogel[65]. Regardless of the specific extracellular changes, these data provide insight into kinase signals that control matrix-related maturation, which thus identify new roles for pathways commonly associated with chemically induced maturation of cardiomyocytes. These data also highlight how sensitive the mechanical induction of these pathways is: LMW PEGDA/HA hydrogels are unable to induce sarcomere assembly likely because they do not sufficiently activate AKT and Wnt pathways. Thus the HMW PEGDA/HA hydrogels, which more closely match how mechanical properties gradually increase during development[16,19], would appear to sufficiently activate these pathways at the right time. With respect to timing however, it is important to note that the sampling rate was sufficient to observe large changes with time but the resolution to capture subtle changes in these pathways may not have been sufficient, i.e. pathways influencing cardiogenesis cycle from being inactive to active throughout

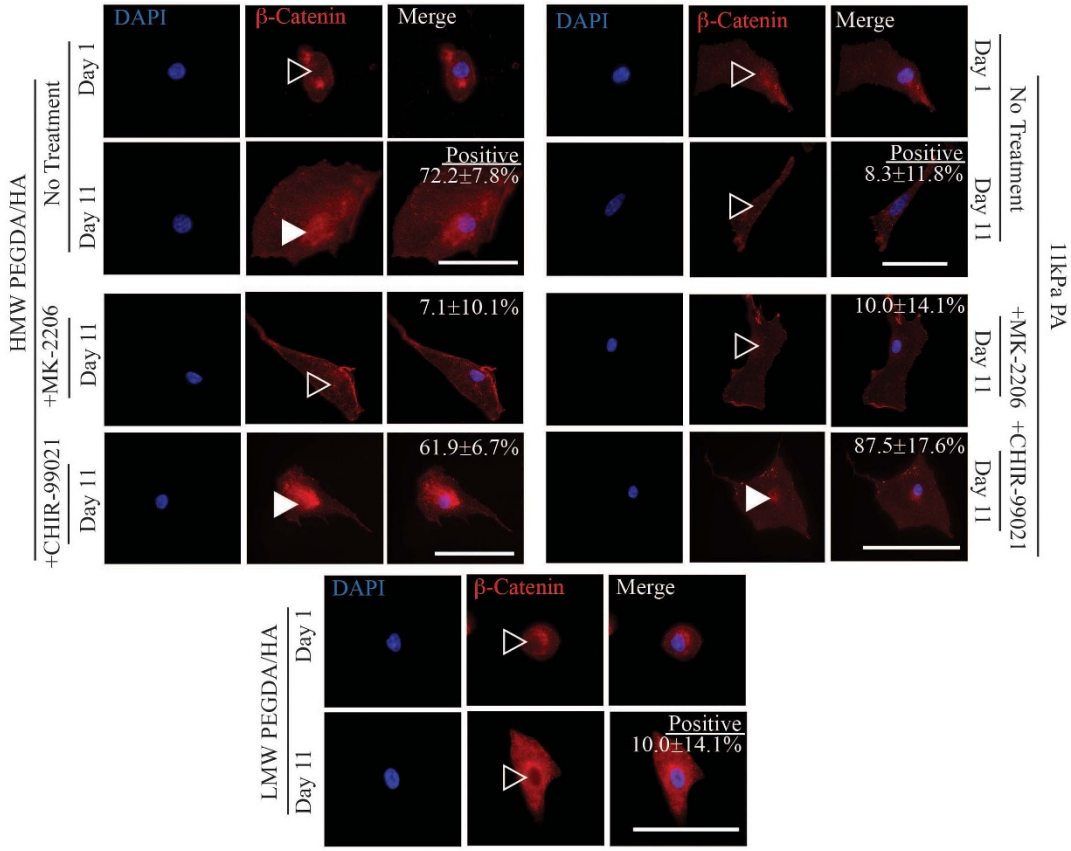

Figure 7 | Localization of β-Catenin Corresponds to Cell State. Cells fixed and stained for β-Catenin (red) and DAPI (blue) are shown for the indicated culture times, treatments, and matrix support types. Open or closed arrowheads highlight diffuse or nuclear localized staining, respectively. At day 11, numbers indicate the percentage of the population with a nuclear localized staining pattern, with error shown from technical replicates. Scale bars = 50 μm.

development[69]. For example, LMW PEGDA/HA hydrogels and stiff PA hydrogels could have also induced some but not all of the sarcomere assembly signals to fully form mature sarcomeres. One final caveat to kinase signaling assays here is that they observe intermediate changes within pathways, i.e. they do not capture the initial signals that change mechanical signals into chemical ones such as kinase cascades. Since much of the cardiac literature has examined how the precise spatial and temporal patterning of protein kinases regulates differentiation[24,25], we focused our assays on kinase signaling. That said, significant efforts to understand focal adhesion protein signaling in this context, e.g. conformational changes in focal adhesion proteins to initial kinase signaling[1,2], are required to further develop our link between the initiation of mechano-sensitive signaling to the propagation of those signals with kinases in cardiomyocytes.

Methods

Hydrogel polymerization. Hyaluronic Acid (HA) hydrogels were prepared in two formulations-with low molecular weight (LMW) and high molecular weight (HMW) poly(ethylene glycol) diacrylate (PEGDA)-in order to achieve hydrogels of different stiffness. To prepare HA hydrogels of the appropriate stiffness to mimic heart stiffening, 4.53% (w/v) HMW PEGDA (BioTime, CA) of ~3.4 kDa (polydispersity index or PDI ~ 3) in degassed phosphate buffered saline (DG PBS) and 1.25% thiolated HA (HA-SH, BioTime, CA) in DG PBS were separately mixed at 37°C with gentle shaking for up to 30 min. Thiolated HA was analyzed via ^{1}H nuclear magnetic resonance (NMR) spectroscopy (ECA 500, JEOL) to assess thiol substitution (~40%). To initiate polymerization, solutions were combined at a 1 : 4 volume ratio of PEGDA to HA to yield a 1% HA/0.9% PEGDA hydrogel. The solution was allowed to polymerize in a humidified 37°C incubator for at least 30 min between aminosilanated and non-adhesive hydroxylated glass coverslips as described elsewhere[66]. Similarly for the preparation of soft HA hydrogels, LMW PEGDA (475629, Sigma, M_n ~ 250) was mixed with 1% thiolated HA at 0.069% and allowed to polymerize for ~30 min at 37°C. To attach protein to the hydrogel surface, 20 mM EDC (ThermoScientific), 50 mM NHS (ThermoScientific) and 150 μg/mL type I rat tail collagen (BD Biosciences) were mixed in PBS and incubated with the hydrogels overnight. Polyacrylamide hydrogels (PA) were prepared as described previously[66]. Briefly, hydrogel crosslinker n,n′-methylene-bis-acrylamide and acrylamide monomer (Fisher Scientific) concentrations were varied in PBS and polymerized between adhesive, aminosilanated and non-adhesive hydroxylated glass coverslips using 1/200 volume of 10% ammonium persulfate (Sigma) and 1/2000 volume of *n*,*n*,*n*′,*n*′-tetramethylethylenediamine (TEMED, BioRad) in order to create hydrogels of defined Young's Modulus, *E*, according to a previously published protocol[66]. To attach protein to the PA hydrogel surface, 0.5 mg/ml of the photo-activating crosslinker, sulfo-SANPAH (Pierce), was mixed in 50 mM HEPES (EMD) of pH 8.5 and activated with 350 nm UV light for 10 min. Type I Collagen (BD Biosciences) was added as with HA hydrogels overnight.

Cell isolation and culture. Animals received humane care in compliance with University of California, San Diego's Institutional Animal Care and Use Committee (protocol #S09200). Chicken embryos were obtained from McIntyre Poultry Farm (Lakeside, CA) and embryonic hearts were obtained by isolation at 72, 120, 168, 240, 312 and 336 hours post-fertilization (HPF) as indicated. Embryo age was confirmed using Hamburger–Hamilton's developmental stages of the chick embryo[37]. Hearts were obtained by dissection and digested for cell isolation. Isolated hearts were minced using sterile razor blades and collected with 10 mL of 0.05% trypsin-EDTA (Invitrogen) and incubated in a sterile humidified 37°C incubator (5% CO_2) for 10 min. In order to remove red blood cells, the tube was inverted and tissue was allowed to settle prior to a change of solution to another 10 mL of fresh trypsin. After incubation for 10 min, the sample was centrifuged at 500 g for 2.5 min and the pellet was carefully triturated with normal heart medium (89% MEM-alpha: l-glutamine (+), ribo-/deoxyribo-nucelosides (−), Invitrogen; 10% fetal bovine serum, Hyclone; and 1% penicilin:streptomycin, Invitrogen). The cell solution was passed through a 70 μm cell strainer (BD Falcon) and pre-plated on tissue culture dishes for 1 hr at 37°C in order to remove fibroblasts from the solution. Unattached cells, which represent the cardiomyocyte fraction[67], were collected, counted, and re-plated at a density of 1–2 × 10^6 cells/mm^2. Overall, myocytes accounted for most cells based on pre-plating and staining. For inhibition experiments, AKT inhibitor (MK-2206, SelleckChem) or GSK3β inhibitor (CHIR-99021, SelleckChem) were added to the media every 2 days at 100 nM from the outset of the experiment. Cells were selectively lysed as described below to monitor targeted protein inhibition via western blotting. Cells used for western blotting were incubated for 1, 3, 5 and 11 days (total age: 96, 144, 192 and 336 HPF, respectively) on HA and 11 kPa PA hydrogels. Cells used for microarray assays were cultured on HA and PA hydrogels for the same time course, in

addition to a 336 HPF sample isolated from the animal as described above. Cells used for immunofluorescence were plated on HA hydrogels and PA hydrogels of 1, 11, and 34 kPa for 1 and 11 days, and on HA and 11 kPa PA hydrogels for the same time course for calcium imaging. Media changes were performed every 2 days. All cell culture and tissue experiments were performed at least in triplicate as indicated.

Protein kinase microarray and analysis. For microarray assays, cells were washed twice in ice cold PBS and lysed in a buffer containing 20 mM MOPS (Fisher Scientific) pH 7.0, 2 mM EGTA (EMD Biosciences), 5 mM EDTA (EMD Biosciences), 30 mM sodium fluoride (J.T. Baker), 60 mM β-glycerophosphate (Sigma), pH 7.2, 20 mM sodium pyrophosphate (Fisher Scientific), 1 mM sodium orthovanadate (Sigma), and 1% Triton X-100 (Fisher Scientific). Two Roche Complete Mini Inhibitor Cocktail tablets (Roche)/10 mL buffer and 1 mM dithiothreitol (DTT, Amresco, OH) were added to the buffer just prior to use. Lysates were sonicated four times for 10 seconds each time with 10–15 second intervals on ice in order to rupture the cells and to shear nuclear DNA. The homogenate was centrifuged at 90,000 × g for 30 min at 4°C in a Beckman Table Top TL-100 ultracentrifuge and the resulting supernatant fraction was analyzed for protein concentration using a commercial Bradford assay reagent (BioRad).

For the Kinex™ Antibody Microarray analyses, a single dye, non-competitive sample binding methodology was used. The array employed 810 polyclonal and monoclonal antibodies (array list available at: http://www.kinexus.ca). Arrays contained 530 pan-specific antibodies (for protein expression) and 280 phosphorylation site-specific antibodies; with overlap in the dataset, 309 unique proteins were examined. For each sample, the microarray chip contained a field of 16 sub-grids, with each grid containing 10 × 11 antibody spots of diameter 120–150 μm. To briefly describe how the microarray was loaded and analyzed, 50 μg of lysate protein from each sample were fluorescently labeled and free dye removed by gel filtration. After blocking for non-specific binding, samples were incubated on the chip, and unbound proteins were subsequently removed with successive washing. Imaging was performed with a Perkin-Elmer ScanArray Reader laser array scanner (Waltham, MA) and signal quantification was performed with *ImaGene 8.0* (BioDiscovery; El Segundo, CA). Z scores were calculated by subtracting average spot intensity within a sample from the raw intensity of each spot and dividing by the spot standard deviation (SD) within each sample[68]. Z ratios were then calculated by taking the difference between the averages of the protein Z scores and dividing by the SD of all of the differences for that particular comparison, e.g. day 3 vs. day 1 HA.

Statistically significant values were determined by performing a 2-way ANOVA with an interaction $p < 0.05$. Clustering was performed using Gene Cluster 3.0 with centroid gene clustering linkage and the resulting heat maps were assembled in Java TreeView. Only those data that were statistically significant as well as at least one time point significantly expressed (z-ratio > 1 or $-1 >$ z-ratio) were visualized in clustering in order to choose the most conservative dataset (Supplemental Table 1). GO-ELITE analysis[39,69] was performed on the statistically significant dataset (not the further reduced set) in order to identity those signaling pathways[38] that were significantly and differentially over-expressed or phosphorylated. Significant pathways were edited using PathVisio software, again using the statistically significant dataset.

Protein array validation via western blotting. Microarray data was validated by performing western blots on a select set of proteins determined by GO ELITE to be in cardiomyocyte relevant pathways that were both statistically significantly and differentially expressed. For western blots, cells still bound to their hydrogels were washed twice in PBS and lysed with mRIPA containing 1% Triton-X (Fisher Scientific), 1% Sodium Deoxycholate (Sigma), 0.1% sodium dodecyl sulfate (Fisher Scientific), 150 mM Sodium Chloride (Fisher Scientific), 10% glycerol (Fisher Scientific), 1.5 mM Magnesium Chloride (Fisher Scientific), 50 mM Hepes (EMD), and pH adjusted to 7.5. Just before use 1 mM Phenylmethylsulfonyl fluoride (EMD), 1 mM Ethylenediaminetetraacetic acid (EMD), and 1% Phosphatase Inhibitor Cocktail B (sc-45045, Santa Cruz Biotechnology) were also added to the buffer. Upon lysis, samples were prepared such that the loading solution consisted of 1/3 volume protein loading dye (National Diagnostics), and were subsequently heated at 90°C for 2 min, and loaded into 10% resolving/5% stacking acrylamide hydrogels and subjected to an electrophoretic gradient for 45 min to 1 hr at 150 V in 10% SDS buffer containing 25 mM Tris (Fisher Scientific), 192 mM Glycine (J.T. Baker) and 20% v/v Methanol (Fisher Scientific). Separated proteins were transferred onto nitrocellulose membrane for 1 hr 15 min at 100 V at 4°C and blocked overnight in blocking buffer containing 1% non-fat milk or 4% Sea-block (ThermoScientific), 25 mM Tris (Fisher Scientific), 150 mM NaCl (Fisher Scientific), and 0.1% Tween-20 (Fisher Scientific). The following antibodies were added to blocking buffer: Paxillin – 1 hr, 1 : 1000 (MBS470022, MyBioSource); AKT1 – 1 hr, 1 : 1000 (AP09425PU-N, Acris Antibodies); AKT2 - 1 hr, 1 : 5000 (AP03032PU-N, Acris Antibodies); GSK3β – overnight at 4°C, 1 : 1000 (ADI-KAM-ST002, Enzo Life Sciences, Inc.); GAPDH – overnight at 4°C, 1 : 1000 (MAB374, Milipore). Upon rinsing, the following HRP-conjugated secondary antibodies were added for 1 hr, depending on the primary antigen: goat anti-rabbit 1 : 10000 (170-6515, BioRad); donkey anti-sheep 1 : 10000 (713-035-003, Jackson); or goat anti-mouse 1 : 10000 (115-035-062, Jackson). Films were exposed using ECL reagent (Thermo Scientific) and processed in a Konica Minolta SRX-101A x-ray developer for 30 sec, 5 min, or 1 hr. All westerns were run in triplicate and quantified using ImageJ, normalized to GAPDH expression except where BCA assays were used for normalization as indicated.

Immunofluorescence assays. In order to examine cell maturation from the time course previously described, immunofluorescence of myofibril development and beta-catenin localization, as well as calcium imaging were performed. For immunofluorescence, cells were fixed with 3.7% formaldehyde in PBS for 30 min, rinsed, and permeabilized using 1% w/v Triton X-100 for 10 min. For myofibrils, cells were rinsed and incubated with primary mouse antibody for α-actinin (A7811, Sigma) at 1 : 500 in 2% ovalbumin (Sigma) for 60 min at 37°C. Samples were then incubated with 1 : 1000 rhodamine-phallodin (R415, Invitrogen) and 1 : 1000 Alexa Flour 488 conjugated goat anti-mouse secondary antibody (A11001, Invitrogen) in 2% ovalbumin for 30 min, followed by 1 : 5000 Hoescht (33342, Sigma) in DH_20 for 10 min at 37°C. For beta catenin localization, cells were stained as above, except that primary rabbit antibody for beta-catenin (ab6302, Abcam) and secondary Alexa Flour 488 conjugated goat anti-rabbit antibody (A11008, Invitrogen) were used at 1 : 1000. A secondary Alexa Fluor 647 conjugated goat anti-mouse antibody (A21235, Invitrogen) was also used for to stain the α-actinin antibody at 1 : 1000. Samples were rinsed and mounted with Fluoromount-G (SouthernBiotech). Images were captured using a 60 × water objective on a Nikon Eclipse TE2000-U fluorescent microscope with a CARVII confocal attachment (Becton Dickenson) and Metamorph 7.6 software. Images were analyzed using ImageJ to determine striation length by drawing a calibrated line through assembled myofibrils within a cell. At least 12 cells were analyzed for cells in culture on PA and HA hydrogels after 1 and 11 days, resulting in analysis of between 46 and 145 myofibrils. For CHIR-treated cells after 11 days in culture on PA and HA hydrogels, at least 9 cells representing between 55 and 87 myofibrils, were analyzed. For MK-2206-treated cells after 11 days in culture on PA and HA hydrogels which had reduced viability, 8 and 4 cells representing 84 and 25 myofibrils, respectively, were analyzed.

Calcium handling assay. Calcium imaging was performed at days 1 and 11 after plating by adding Fluo-4 AM (F-14201, Invitrogen) at 1 : 2000 directly to the media for 10 minutes. Videos were captured using a Nikon Eclipse TE2000-U fluorescent microscope outfitted with a LiveCell imager with Metamorph 7.6 software. Videos were analyzed in MATLAB using custom-written code to determine the power spectral density and frequency of the signal using a Fourier Transform-based analysis[34].

Statistical analyses. Microarray and western blot validation statistical analyses were performed using a 2-way ANOVA. Differences among groups were assessed to identify statistical differences between the interaction of hydrogel types and time points when $p < 0.05$. All other statistical analyses were performed using student t-tests or 1-way ANOVA as indicated. Differences among groups were assessed to identify statistical differences between treatments when $p < 0.05$. All data is presented as mean ± standard deviation from triplicate biological experiments except those within the microarray, which were performed in duplicate, or when otherwise indicated.

1. Engler, A. J., Sen, S., Sweeney, H. L. & Discher, D. E. Matrix Elasticity Directs Stem Cell Lineage Specification. *Cell* **126**, 677–689 (2006).
2. Saha, K. *et al.* Substrate Modulus Directs Neural Stem Cell Behavior. *Biophys J* **95**, 4426–4438 (2008).
3. Holle, A. W. & Engler, A. J. More than a feeling: discovering, understanding, and influencing mechanosensing pathways. *Curr Op Biotechnol* **22**, 648–654 (2011).
4. Wang, W. *et al.* Tumor cells caught in the act of invading: their strategy for enhanced cell motility. *Trends Cell Biol* **15**, 138–145 (2005).
5. Hay, E. D. *Cell biology of extracellular matrix* Hay, E. D. (ed.) xv–417 (Plenum Press, New York, 1981).
6. Nelson, C. M. & Bissell, M. J. Of extracellular matrix, scaffolds, and signaling: tissue architecture regulates development, homeostasis, and cancer. *Annu Rev Cell Dev Biol.* **22**, 287–309 (2006).
7. Montell, D. J. Morphogenetic cell movements: diversity from modular mechanical properties. *Science* **322**, 1502–1505 (2008).
8. Jacot, J. G., McCulloch, A. D. & Omens, J. H. Substrate stiffness affects the functional maturation of neonatal rat ventricular myocytes. *Biophys J* **95**, 3479–3487 (2008).
9. Engler, A. J. *et al.* Embryonic cardiomyocytes beat best on a matrix with heart-like elasticity: scar-like rigidity inhibits beating. *J Cell Sci* **121**, 3794–3802 (2008).
10. Peyton, S. R. & Putnam, A. J. Extracellular matrix rigidity governs smooth muscle cell motility in a biphasic fashion. *J Cell Physiol* **204**, 198–209 (2005).
11. Zaari, N., Rajagopalan, P., Kim, S. K., Engler, A. J. & Wong, J. Y. Photopolymerization in Microfluidic Gradient Generators: Microscale Control of Substrate Compliance to Manipulate Cell Response. *Adv Mater* **16**, 2133–2137 (2004).
12. Huebsch, N. *et al.* Harnessing traction-mediated manipulation of the cell/matrix interface to control stem-cell fate. *Nature Mater* **9**, 518–526 (2010).
13. Shih, Y.-R. V., Tseng, K.-F., Lai, H.-Y., Lin, C.-H. & Lee, O. K. Matrix stiffness regulation of integrin-mediated mechanotransduction during osteogenic differentiation of human mesenchymal stem cells. *J Bone Miner Res* **26**, 730–738 (2011).
14. Ghosh, K. *et al.* Cell adaptation to a physiologically relevant ECM mimic with different viscoelastic properties. *Biomaterials* **28**, 671–679 (2007).
15. Marklein, R. A. & Burdick, J. A. Spatially controlled hydrogel mechanics to modulate stem cell interactions. *Soft Matter* **6**, 136–143 (2010).

16. Young, J. L. & Engler, A. J. Hydrogels with time-dependent material properties enhance cardiomyocyte differentiation in vitro. *Biomaterials* **32**, 1002–1009 (2011).
17. Lutolf, M. P. & hubbell, J. A. Synthetic biomaterials as instructive extracellular microenvironments for morphogenesis in tissue engineering. *Nature Biotechnol* **23**, 47–55 (2005).
18. Deroanne, C. F., Lapiere, C. M. & Nusgens, B. V. In vitro tubulogenesis of endothelial cells by relaxation of the coupling extracellular matrix-cytoskeleton. *Cardiovasc Res* **49**, 647–658 (2001).
19. Jacot, J. G., Martin, J. C. & Hunt, D. L. Mechanobiology of cardiomyocyte development. *J Biomech* **43**, 93–98 (2010).
20. Discher, D. E., Mooney, D. J. & Zandstra, P. W. Growth factors, matrices, and forces combine and control stem cells. *Science* **324**, 1673–1677 (2009).
21. Berry, M. F. *et al.* Mesenchymal stem cell injection after myocardial infarction improves myocardial compliance. *Am J Physiol Heart Circ Physiol* **290**, H2196–203 (2006).
22. Krieg, M. *et al.* Tensile forces govern germ-layer organization in zebrafish. *Nature* **10**, 429–436 (2008).
23. Zamir, E. A. & Taber, L. A. Material Properties and Residual Stress in the Stage 12 Chick Heart During Cardiac Looping. *J Biomech Eng* **126**, 823–830 (2004).
24. Wagner, M. & Siddiqui, M. A. Q. Signal Transduction in Early Heart Development (I): Cardiogenic Induction and Heart Tube Formation. *Exp Biol Med* **232**, 852–865 (2007).
25. Wagner, M. & Siddiqui, M. A. Q. Signal Transduction in Early Heart Development (II): Ventricular Chamber Specification, Trabeculation, and Heart Valve Formation. *Exp Biol Med* **232**, 866–880 (2007).
26. Bottcher, R. T. Fibroblast Growth Factor Signaling during Early Vertebrate Development. *Endocr Rev* **26**, 63–77 (2005).
27. Dailey, L., Ambrosetti, D., Mansukhani, A. & Basilico, C. Mechanisms underlying differential responses to FGF signaling. *Cytokine Growth Factor Rev* **16**, 233–247 (2005).
28. Sheldahl, L. C. *et al.* Dishevelled activates Ca2+ flux, PKC, and CamKII in vertebrate embryos. *J Cell Biol* **161**, 769–777 (2003).
29. Pandur, P., Läsche, M., Eisenberg, L. M. & Kühl, M. Wnt-11 activation of a non-canonical Wnt signalling pathway is required for cardiogenesis. *Nature* **418**, 636–641 (2002).
30. Schneider, V. A. & Mercola, M. Wnt antagonism initiates cardiogenesis in Xenopus laevis. *Genes Dev* **15**, 304–315 (2001).
31. Naito, A. T. *et al.* Phosphatidylinositol 3-Kinase–Akt Pathway Plays a Critical Role in Early Cardiomyogenesis by Regulating Canonical Wnt Signaling. *Circ Res* **97**, 144–151 (2005).
32. Allen, D. G. & Kentish, J. C. The cellular basis of the length-tension relation in cardiac muscle. *J Mol Cell Cardiol* **17**, 821–840 (1985).
33. Gomez, J.-P., Potreau, D. & Raymond, G. Intracellular calcium transients from newborn rat cardiomyocytes in primary culture. *Cell Calcium* **15**, 265–275 (1994).
34. Bu, G., Adams, H., Berbari, E. J. & Rubart, M. Uniform Action Potential Repolarization within the Sarcolemma of In Situ Ventricular Cardiomyocytes. *Biophys J* **96**, 2532–2546 (2009).
35. McCain, M. L. & Parker, K. K. Mechanotransduction: the role of mechanical stress, myocyte shape, and cytoskeletal architecture on cardiac function. *Pflugers Arch* **462**, 89–104 (2011).
36. Sanger, J. W., Wang, J., Fan, Y., White, J. & Sanger, J. M. Assembly and Dynamics of Myofibrils. *J Biomed Biotech* **2010**, 1–8 (2010).
37. Hamburger, V. & Hamilton, H. L. A series of normal stages in the development of the chick embryo. *Dev Dyn* **195**, 231–272 (1992).
38. Pico, A. R. *et al.* WikiPathways: Pathway Editing for the People. *PLoS Biol* **6**, e184 (2008).
39. Zambon, A. C. *et al.* GO-Elite: a flexible solution for pathway and ontology over-representation. *Bioinformatics* **28**, 2209–2210 (2012).
40. Sussman, M. A. *et al.* Myocardial AKT: The Omnipresent Nexus. *Physiol Rev* **91**, 1023–1070 (2011).
41. Kerkela, R. *et al.* Deletion of GSK-3β in mice leads to hypertrophic cardiomyopathy secondary to cardiomyoblast hyperproliferation. *J Clin Invest* **118**, 3609 (2008).
42. Sero, J. E. *et al.* Paxillin Mediates Sensing of Physical Cues and Regulates Directional Cell Motility by Controlling Lamellipodia Positioning. *PLoS ONE* **6**, e28303 (2011).
43. Alon, R. *et al.* α4β1-dependent adhesion strengthening under mechanical strain is regulated by paxillin association with the α4-cytoplasmic domain. *J Cell Biol* **171**, 1073–1084 (2005).
44. Fujio, Y., Nguyen, T., Wencker, D., Kitsis, R. N. & Walsh, K. Akt Promotes Survival of Cardiomyocytes In Vitro and Protects Against Ischemia-Reperfusion Injury in Mouse Heart. *Circ* **101**, 660–667 (2000).
45. Pelham, R. J. & Wang, Y.-L. Cell locomotion and focal adhesions are regulated by substrate flexibility. *PNAS* **94**, 13661–13665 (1997).
46. Rafalski, V. A. *et al.* Expansion of oligodendrocyte progenitor cells following SIRT1 inactivation in the adult brain. *Nature* **15**, 614–624 (2013).
47. Ring, D. B. *et al.* Selective Glycogen Synthase Kinase 3 Inhibitors Potentiate Insulin Activation of Glucose Transport and Utilization In Vitro and In Vivo. *Diabetes* **52**, 588–595 (2003).
48. Collignon, J., Varlet, I. & Robertson, E. J. Relationship between asymmetric nodal expression and the direction of embryonic turning. *Nature* **381**, 155–158 (1996).
49. Boettger, T., Wittler, L. & Kessel, M. FGF8 functions in the specification of the right body side of the chick. *Curr Biol* **9**, 277–280 (1999).
50. Ramsdell, A. F. & Yost, H. J. Cardiac looping and the vertebrate left-right axis: antagonism of left-sided Vg1 activity by a right-sided ALK2-dependent BMP pathway. *Dev* **126**, 5195–205 (1999).
51. Voronov, D. A., Alford, P. W., Xu, G. & Taber, L. A. The role of mechanical forces in dextral rotation during cardiac looping in the chick embryo. *Dev Biol* **272**, 339–350 (2004).
52. Tobita, K., Schroder, E. A., Tinney, J. P., Garrison, J. B. & B, K. B. Regional passive ventricular stress-strain relations during development of altered loads in chick embryo. *Am J Physiol Heart Circ Physiol* **282**, H2386–H2396 (2002).
53. Miller, C. E., Vanni, M. A., Taber, L. A. & B, K. B. Passive stress-strain measurements in the stage-16 and stage-18 embryonic chick heart. *J Biomech Eng* **119**, 445–451 (1997).
54. Hanson, K. P. *et al.* Spatial and Temporal Analysis of Extracellular Matrix Proteins in the Developing Murine Heart: A Blueprint for Regeneration. *Tissue Eng Pt A* **19**, 1132–1143 (2013).
55. Gittenberger-De Groot, A. C. *et al.* Collagen type VI expression during cardiac development and in human fetuses with trisomy 21. *Anat Rec* **275A**, 1109–1116 (2003).
56. Bajaj, P., Tang, X., Saif, T. A. & Bashir, R. Stiffness of the substrate influences the phenotype of embryonic chicken cardiac myocytes. *J Biomed Mater Res* **95A**, 1261–1269 (2010).
57. Poobalarahi, F., Baicu, C. F. & Bradshaw, A. D. Cardiac myofibroblasts differentiated in 3D culture exhibit distinct changes in collagen I production, processing, and matrix deposition. *Am J Physiol Heart Circ Physiol* **291**, H2924–H2932 (2006).
58. van Laake, L. W. *et al.* Extracellular matrix formation after transplantation of human embryonic stem cell-derived cardiomyocytes. *Cell Mol Life Sci* **67**, 277–290 (2010).
59. Pontes Soares, C. *et al.* 2D and 3D-organized cardiac cells shows differences in cellular morphology, adhesion junctions, presence of myofibrils and protein expression. *PLoS ONE* **7**, e38147 (2012).
60. Tiburcy, M. *et al.* Terminal Differentiation, Advanced Organotypic Maturation, and Modeling of Hypertrophic Growth in Engineered Heart Tissue. *Circ Res* **109**, 1105–1114 (2011).
61. McBeath, R., Pirone, D. M., Nelson, C. M., Bhadriraju, K. & Chen, C. S. Cell Shape, Cytoskeletal Tension, and RhoA Regulate Stem Cell Lineage Commitment. *Dev Cell* **6**, 483–495 (2004).
62. Lian, X. *et al.* Directed cardiomyocyte differentiation from human pluripotent stem cells by modulating Wnt/β-catenin signaling under fully defined conditions. *Nature Protoc* **8**, 162–175.
63. Haq, S. *et al.* Differential Activation of Signal Transduction Pathways in Human Hearts With Hypertrophy Versus Advanced Heart Failure. *Circ* **103**, 670–677 (2001).
64. Breitbach, M. *et al.* Potential risks of bone marrow cell transplantation into infarcted hearts. *Blood* **110**, 1362–1369 (2007).
65. Trappmann, B. *et al.* Extracellular-matrix tethering regulates stem-cell fate. *Nature Mater* **11**, 642–649 (2012).
66. Tse, J. R. & Engler, A. J. Preparation of hydrogel substrates with tunable mechanical properties. *Curr Protoc Cell Biol* **47**, 10.16.1–10.16.16 (2010).
67. Dabiri, G. A., Ayoob, J. C., Turnacioglu, K. K., Sanger, J. M. & Sanger, J. W. Use of green fluorescent proteins linked to cytoskeletal proteins to analyze myofibrillogenesis in living cells. *Methods in Enzymology* Conn, M. (ed.) 171–186 (Elsevier, New York, 1999).
68. Cheadle, C., Vawter, M. P., Freed, W. J. & Becker, K. G. Analysis of Microarray Data Using Z Score Transformation. *J Mol Diagn* **5**, 73–81 (2010).
69. Botstein, D. *et al.* Gene Ontology: tool for the unification of biology. *Nature Genet* **25**, 25–29 (2000).

Acknowledgments

This work was supported by grants from the American Heart Association (0865150F to A.J.E. and SDG2630130 to A.C.Z.), National Institutes of Health (R21HL106529 to A.J.E. and 1U54HK08460 A.C.Z.), American Heart Association Pre-Doctoral Fellowship (10PRE4160143 to J.L.Y.), National Science Foundation Graduate Research Fellowship (to M.G.O.), Achievement Rewards for College Scientists Fellowship (ARCS; to J.L.Y.) and California Institute for Regenerative Medicine (CIRM) Bridges Program (TB1-01186 to K.K.). The authors would also like acknowledge Dr. Gretchen A. Meyer for use of her MATLAB code in analyzing calcium imaging data.

Author contributions

J.L.Y., K.K., A.C.Z. and A.J.E. designed the research. J.L.Y., K.K. and M.G.O. performed the research. J.L.Y., K.K. and M.G.O. analyzed the data. J.L.Y., A.C.Z. and A.J.E. wrote the paper.

Additional information

Supplementary information accompanies this paper at http://www.nature.com/scientificreports

Competing financial interests: The authors declare no competing financial interests.

How to cite this article: Young, J.L., Kretchmer, K., Ondeck, M.G., Zambon, A.C. & Engler, A.J. Mechanosensitive Kinases Regulate Stiffness-Induced Cardiomyocyte Maturation. *Sci. Rep.* **4**, 6425; DOI:10.1038/srep06425 (2014).